European Journal of Mechanics / A Solids 105 (2024) 105274

Contents lists available at ScienceDirect

European Journal of Mechanics / A Solids

journal homepage: www.elsevier.com/locate/ejmsol

Full length article

A closed-form solution for evaluating the *Findley* critical plane factor

A. Chiocca *, M. Sgamma, F. Frendo

Department of Civil and Industrial Engineering, University of Pisa, Pisa, Italy

ARTICLE INFO

Keywords:
Critical plane
Findley
Material fatigue
Computational efficiency
Algorithm optimization

ABSTRACT

The fatigue assessment of structural components is a significant topic investigated both in the academia and industry. Despite the significant progress in comprehension over the past few decades, fatigue damage remains a significant challenge, often leading to unexpected component failures. One commonly used approach for fatigue assessment is the critical plane analysis, which aids in identifying the critical location and early crack propagation direction in a component. However, the conventional method for calculating critical plane factors is computationally demanding and is typically utilized only when the critical regions of the component are already known. In situations where the critical areas are difficult to be identified due to complex geometry, loads, or constraints, a more efficient method is required for evaluating critical plane factors. This research paper introduces an analytical algorithm to efficiently evaluates the widely used *Findley* critical plane factor. The algorithm operates within the framework of linear-elastic material behavior and proportional loading conditions, relying on tensor invariants and coordinate transformation laws. The algorithm has been tested on different component geometries, including a box-welded joint and a tubular specimen, subjected to proportional loading conditions such as tension, torsion, and a combination of them. The analytical method allowed a significant reduction in computation time while providing the exact solution of critical plane factor and critical plane orientations.

1. Introduction

The investigation of fatigue damage in materials is a strategic topic in various fields, including academia and industry. Cyclic loading during operation remains a leading cause of unforeseen failures and a critical challenge for designers (Bhaumik et al., 2008). While fatigue tests typically represent simplified scenarios, complications such as stress/strain gradients, variable amplitude loading, randomness, multiaxiality and residual stresses can arise in practical cases (Kuncham et al., 2022; Chiocca et al., 2022). In such circumstances, finite element analysis (FEA) is a valuable tool that can consider the complex characteristics discussed above (Chen et al., 2022; Frendo et al., 2020; Chiocca et al., 2019; Tamburrino et al., 2023; Chiocca et al., 2021; Fontana et al., 2023). Traditionally, fatigue analysis involves studying the critical regions of a component (i.e. taking into account stress/strain gradients and multiaxiality) and applying the appropriate loading history (i.e. accounting for variable amplitude or randomness) (Sgamma et al., 2023; Sharma and Hiremath, 2023; Wang and Yim, 2023). Nevertheless, due to the vast array of geometries, loading conditions, and damage parameters that must be considered, solving such models can be time-consuming during both the solution and post-processing phases. While the complexity of the geometry and boundary conditions is intrinsically linked to the problem being investigated and thus unavoidable, the selection of the damage parameter is ultimately up to the designer. Several techniques exist for evaluating fatigue damage (Lazzarin and Berto, 2005; Berto and Lazzarin, 2009; Mroziński, 2019; Varvani-Farahani et al., 2007; European Committee for Standardization (CEN), 2005; Hobbacher, 2009; Karakaş et al., 2018; Braccesi et al., 2018; Morettini et al., 2020, 2021; Taylor et al., 2002; Radaj et al., 2006; Campagnolo et al., 2017; Mirzaei et al., 2023; Fatemi and Socie, 1988; Findley, 1959; Kandil et al., 1982; Socie, 1987). Within this framework and in the context of local damage techniques, critical plane factor (CP) methods are recognized to be among the most promising approaches (Huang et al., 2014; Reis et al., 2014; Cruces et al., 2018; El-sayed et al., 2018; Cruces et al., 2022). Damage methods that rely on critical plane entail determining the plane orientation that experiences the most severe damage. This plane is referred to as the critical plane and represents the local specific orientation over which the crack should initially nucleate and propagate (Arora et al., 2021). Particularly for implementing such damage parameters, FEM is highly advantageous when dealing with intricate geometries and complex loading histories. The conventional method for evaluating both the critical plane factor and orientation necessitates computing the damage factor on all possible plane orientations in space. The critical

* Corresponding author.
E-mail addresses: andrea.chiocca@unipi.it (A. Chiocca), michele.sgamma@phd.unipi.it (M. Sgamma), francesco.frendo@unipi.it (F. Frendo).

https://doi.org/10.1016/j.euromechsol.2024.105274
Received 18 December 2023; Received in revised form 24 January 2024; Accepted 19 February 2024
Available online 23 February 2024

plane (i.e. the one that identifies the maximum value of the damage parameter) is determined by performing an iterative plane scanning process over all orientations in space, with a given spatial resolution. The plane orientation can be identified by two angles, which are varied discretely by an angular step to cover all three-dimensional space. The process has to be performed for each node of the FE-model, generally utilizing nested *for/end* loops, which requires significant computational power. However, despite the potential benefits of these methodologies, their implementation remains computationally challenging, which limits their applicability. In comparison to other widely used damage factors, such as nominal stress, hot spot stress, and notch stress approach, the critical plane method is still mostly confined to research and academia and has yet to gain widespread acceptance in industry. The current extensive computation time involved in evaluating the critical plane factor restricts the direct examination of only the critical zone of a component (e.g., notch). However, this area may not always be identifiable *a priori* due to the complexity of geometries, load histories, and constraints (Chiocca et al., 2023c, 2024).

During the computational process, it can be challenging to balance accuracy and efficiency by choosing the appropriate angular increment for iteration. To reduce the time needed for critical plane factor calculations, previous research has focused on using analytical or semi-analytical techniques. Marques et al. (2020) proposed a new algorithm that utilizes analytical formulas to determine solely the spectral parameters relevant to the damage factor. On the other hand, some alternative methods focus on enhancing computational efficiency by computing the critical plane factor solely in certain planes, instead of discretizing the entire three-dimensional space, as presented by Wentingmann et al. (2020) and Sunde et al. (2020). Wentingmann's method segments a coarse Weber half sphere with quad elements while Sunde's method densifies a triangular mesh around the elements where the greatest damage has been observed. Finally, in some cases, the loading condition of the specimen allows for a purely analytical formulation of the damage factor, leading to reduced stress states (Liu et al., 2021; Albinmousa and Al Hussain, 2021; Ma et al., 2022). However, this requires the use of a specific reference frame to obtain such a reduced tensor configuration.

In recent papers (Chiocca et al., 2023a,b, 2024; Sgamma et al., 2024) the authors presented algorithms for efficiently calculating critical plane parameters, such as *Fatemi-Socie*, *Smith–Watson–Topper* or *Kandil–Brown–Miller*. The algorithm implements a closed-form expression for some CP factors and the relative critical plane orientations. In this paper, an analytical approach is introduced to assess the *Findley* critical plane parameter using stress and strain tensor invariants and coordinate transformation laws. The method is designed for linear-elastic material models and proportional loading conditions. The algorithm is intended to be applied for finite element analysis, with a discrete formulation of the time sequence. Stress and strain tensors are defined with respect to the ith *load step*, and for complex loading histories, the method can be iteratively applied to each successive peak-to-valley or valley-to-peak pair from a specific cycle counting formulation. The paper first provides the theoretical basis for the methodology, followed by case studies that include various specimens under different loading conditions. The study compares the novel methodology with the standard plane scanning approach in terms of result's accuracy and computational cost.

2. Critical plane factor evaluation

2.1. Critical plane factor formulation

The following section focuses on introducing the *Findley* CP factor (FI) (Findley, 1959) formulation together with the standard plane scanning method and the closed form solution. The *Findley* CP factor formulation is presented in Eq. (1),

$$FI = \max\left(\Delta\tau + k\sigma_n\right) \tag{1}$$

where $\Delta\tau$ is the range of shear stress, σ_n is the maximum normal stress on the plane being evaluated and k is a material parameter that can be calculated by conducting tests on specimens subjected to uniaxial tensile and torsion loadings (de Freitas et al., 2017). The critical plane factor FI is commonly used to study the material's response to shear loadings.

In a previous paper by the authors (Chiocca et al., 2023a) a general method, valid for any material property and loading condition, was presented for parameters that involves the maximization of a single stress parameter. The FI parameter, instead, involves maximizing a combination of shear stress range and normal stress and this complicates the process of identifying an analytical solution. In fact, as it will be shown, it is necessary to introduce some simplifying assumptions in order to derive a viable closed form formulation.

2.2. Standard plane scanning technique

This section will outline the conventional method for evaluating the CP factor using the plane scanning technique. At each point in the component's volume, represented by nodes or integration points in finite element models, the time-varying stress $\boldsymbol{\sigma}(t)$ and strain $\boldsymbol{\varepsilon}(t)$ tensors can be determined. Once a specific point is chosen, the structural solution is embedded in such tensors, as described in Eq. (2),

$$\boldsymbol{\sigma}(t) = \begin{bmatrix} \sigma_{xx}(t) & \tau_{xy}(t) & \tau_{xz}(t) \\ \tau_{yx}(t) & \sigma_{yy}(t) & \tau_{yz}(t) \\ \tau_{zx}(t) & \tau_{zy}(t) & \sigma_{zz}(t) \end{bmatrix},\ \boldsymbol{\varepsilon}(t) = \begin{bmatrix} \varepsilon_{xx}(t) & \frac{\gamma_{xy}}{2}(t) & \frac{\gamma_{xz}}{2}(t) \\ \frac{\gamma_{yx}}{2}(t) & \varepsilon_{yy}(t) & \frac{\gamma_{yz}}{2}(t) \\ \frac{\gamma_{zx}}{2}(t) & \frac{\gamma_{zy}}{2}(t) & \varepsilon_{zz}(t) \end{bmatrix} \tag{2}$$

Relationships (2) provides stress and strain tensors in a general reference system $Oxyz$; this tensor notation is useful in describing different loading conditions, including uniaxial, biaxial or multiaxial conditions; the loading cycle, in addition, may exhibit proportional or non-proportional stress components, depending on the load histories. To calculate stress and strain values for each direction in space, a plane Γ can be defined through its unit normal vector $\mathbf{n}$ or two angular coordinates θ and ψ, as shown in Fig. 1. By rotating the Γ plane through a fixed angular step (i.e., $\Delta\theta$ and $\Delta\psi$), stress and strain values in all directions can be determined for each rotated plane. The critical plane, which maximizes the reference CP parameter, can then be identified. However, implementing this plane rotation operation requires nested *for/end* loops, which are computationally inefficient and require significant effort, particularly when multiple points of a component have to be analyzed.

In this study, a rotational sequence within a moving reference frame was adopted. The sequence involved an initial rotation denoted as ψ about the z-axis, followed by a subsequent rotation denoted as θ about the y-axis, as illustrated in Eq. (3). To perform the scanning process, it was set an angular increment of 1° on both $\Delta\theta$ and $\Delta\psi$.

$$R = R_z(\psi)R_y(\theta) = \begin{bmatrix} \cos(\theta)\cos(\psi) & -\sin(\psi) & \cos(\psi)\sin(\theta) \\ \sin(\psi)\cos(\theta) & \cos(\psi) & \sin(\theta)\sin(\psi) \\ -\sin(\theta) & 0 & \cos(\theta) \end{bmatrix} \tag{3}$$

Utilizing the rotation matrix denoted as R, it becomes straightforward to define the stress and strain tensors within the rotated reference frame (i.e. $\boldsymbol{\sigma}'$ and $\boldsymbol{\varepsilon}'$), as described in Eq. (4).

$$\boldsymbol{\sigma}' = R^T\boldsymbol{\sigma}R,\ \boldsymbol{\varepsilon}' = R^T\boldsymbol{\varepsilon}R \tag{4}$$

2.3. Formulation of the closed form solution

In order to understand the analytical method, the mathematical framework has to be introduced first. The method considers a discrete formulation of the time sequence, as it is conventional for a finite element analysis, where load steps ith and i+1th are identified at

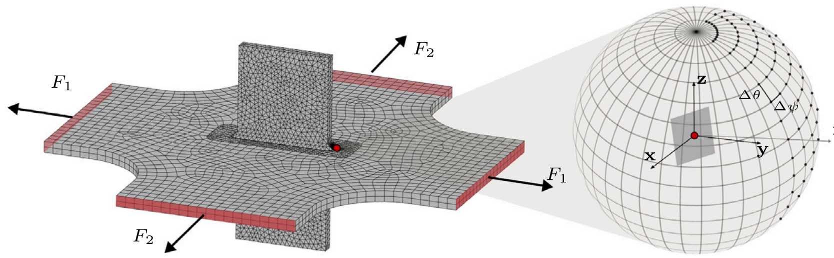

Fig. 1. Sequential plane scanning process used to calculate the critical plane factor and determine the critical plane orientation.

successive times in the load time history. Eq. (5) gives the stress and strain tensors for a generic ith load step.

$$\boldsymbol{\sigma}^{(i)} = \begin{bmatrix} \sigma_{xx} & \tau_{xy} & \tau_{xz} \\ \tau_{yx} & \sigma_{yy} & \tau_{yz} \\ \tau_{zx} & \tau_{zy} & \sigma_{zz} \end{bmatrix}^{(i)}, \ \boldsymbol{\varepsilon}^{(i)} = \begin{bmatrix} \varepsilon_{xx} & \frac{\gamma_{xy}}{2} & \frac{\gamma_{xz}}{2} \\ \frac{\gamma_{yx}}{2} & \varepsilon_{yy} & \frac{\gamma_{yz}}{2} \\ \frac{\gamma_{zx}}{2} & \frac{\gamma_{zy}}{2} & \varepsilon_{zz} \end{bmatrix}^{(i)} \tag{5}$$

The method considers the tensor difference between the ith and $i+1$th load steps, as described in Eq. (6). It is important to note that for mathematical applicability, both tensors must be defined with respect to the same reference frame, but this condition is generally satisfied during the results extraction in the post-processing phase of FE-analyses.

$$\boldsymbol{\Delta\sigma}^{(i,i+1)} = \boldsymbol{\sigma}^{(i)} - \boldsymbol{\sigma}^{(i+1)} = \begin{bmatrix} \Delta\sigma_{xx} & \Delta\tau_{xy} & \Delta\tau_{xz} \\ \Delta\tau_{yx} & \Delta\sigma_{yy} & \Delta\tau_{yz} \\ \Delta\tau_{zx} & \Delta\tau_{zy} & \Delta\sigma_{zz} \end{bmatrix}^{(i,i+1)} \tag{6}$$

In order to apply the proposed method, it is necessary to assume proportional loading condition and liner-elastic material behavior. Under these assumptions, the principal directions do not change between different load steps, that is, the same *eigenvector* associated with a generic *eigenvalue* will be maintained between two successive *load steps* i and $i+1$. Therefore, under such conditions, also $\boldsymbol{\Delta\sigma}^{(i,i+1)}$ will have the same principal directions of $\boldsymbol{\sigma}^{(i)}$ and $\boldsymbol{\sigma}^{(i+1)}$. To further illustrate the method, the Mohr's circular representation will be employed. Fig. 2 provides a graphical representation of the closed form solution using the tensors $\boldsymbol{\Delta\sigma}^{(i,i+1)}$, $\boldsymbol{\sigma}^{(i)}$, and $\boldsymbol{\sigma}^{(i+1)}$, and the Cauchy elementary material volume.

Stress data must first be extracted from a point in the component with respect to a generic reference frame $Oxyz$. Then, an *eigenvalue–eigenvector* analysis is performed on the stress range tensor $\boldsymbol{\Delta\sigma}^{(i,i+1)}$, which yields the principal stress range parameters ($\Delta\sigma_1^{(i,i+1)}$, $\Delta\sigma_2^{(i,i+1)}$, and $\Delta\sigma_3^{(i,i+1)}$) and principal directions $\mathbf{n_1}^{(i),(i+1)}$, $\mathbf{n_2}^{(i),(i+1)}$, and $\mathbf{n_3}^{(i),(i+1)}$. As previously discussed, these directions represent the principal directions of $\boldsymbol{\sigma}^{(i)}$ and $\boldsymbol{\sigma}^{(i+1)}$, as well. The tensors $\boldsymbol{\Delta\sigma}^{(i,i+1)}$, $\boldsymbol{\sigma}^{(i)}$, and $\boldsymbol{\sigma}^{(i+1)}$ expressed in the principal reference frame $On_1n_2n_3$ are then represented by their principal components. The largest magnitude of the FI parameter will be referred to a point in the circular representation belonging to the largest circumference; therefore, the critical orientation can be looked for by rotating about the $\mathbf{n_2}^{(i,i+1)}$ direction by a given angle ω.

Eqs. (7)–(8) present the analytical formulation for $\Delta\tau^{(i,i+1)}(\omega)$ and $\sigma_n(\omega)$ and can be derived from the Mohr's notation by using simple basic trigonometry.

$$\Delta\tau^{(i,i+1)}(\omega) = \left(\frac{\Delta\sigma_1^{(i,i+1)} - \Delta\sigma_3^{(i,i+1)}}{2}\right)\sin(2\omega) \tag{7}$$

$$\sigma_n(\omega) = \max_{\{i,i+1\}}\left[\left(\frac{\sigma_1+\sigma_3}{2}\right) + \left(\frac{\sigma_1-\sigma_3}{2}\right)\cos(2\omega)\right] \tag{8}$$

By substituting Eqs. (7)–(8) into Eq. (1), it is possible to derive an analytical expression of $FI(\omega)$, as shown in Eq. (9)

$$FI(\omega) = \max_{\{\omega\}}\left[\Delta\tau^{(i,i+1)}(\omega) + k\,\sigma_n(\omega)\right] \tag{9}$$

which, after introducing the parameters:

$$\begin{cases} a = \left(\frac{\Delta\sigma_1 - \Delta\sigma_3}{2}\right) \\ b = \left(\frac{\sigma_1+\sigma_3}{2}\right) \\ c = \left(\frac{\sigma_1-\sigma_3}{2}\right) \end{cases} \tag{10}$$

leads to the following maximization problem (i.e., Eq. (11)):

$$FI(\omega) = \max_{\{\omega\}}\left[a\sin(2\omega) + k\,(b + c\cos(2\omega))\right] \tag{11}$$

in terms of the angle ω. By setting to zero the derivative of the given function, the maximum value of *FI* and the relative angle ($\bar{\omega}$) for which it is maximized can be obtained. The solutions in terms of $\bar{\omega}$ and $FI(\bar{\omega})$ are given in the following Eqs. (12)–(13).

$$\bar{\omega} = \frac{1}{2}\arctan\left(\frac{a}{c\ k}\right) \tag{12}$$

$$FI(\bar{\omega}) = b\ k + \sqrt{a^2 + c^2k^2} \tag{13}$$

It is worth noting that, the parameter b represents the center of the largest stress circle and can assume any real value, while a, representing the radius of the largest stress range circle and c, representing the radius of the largest stress circle, are always positive. The limits of a and c are given by the standard convention on the eigenvalues ordering, where the first one is always greater than the consecutive. The functions $\bar{\omega}$ and $FI(\bar{\omega})$ are defined as continuous in the intervals $a = [0,\infty)$, $b = (-\infty,\infty)$, $c = [0,\infty)$, $k = [0,\infty)$. Fig. 3 presents $\bar{\omega}$ and $FI(\bar{\omega})$ over a and b. The c values are step-varied assuming a range of $c = [1,100]$, while the material parameter k has been kept constant at a standard value of $k = 0.3$ for all cases. From Fig. 3a–b it can be seen how b has no effect on the $\bar{\omega}$ formulation, while from Fig. 3c–d it is visible how the effect of the parameter c becomes negligible on the $FI(\bar{\omega})$ function while a increases.

After obtaining the critical plane factor $FI(\bar{\omega})$, it is possible to derive the orientation of the critical plane. This can be achieved by utilizing the rotation matrix specified in Eq. (14). The rotation matrix is obtained by multiplying the matrix R_p, which contains the direct cosines of the principal directions, with the rotation matrix R_y. The rotation matrix R_y represents the rotation about the y-axis by an angle $\bar{\omega}$.

$$R = R_pR_y(\bar{\omega}) = \begin{bmatrix} | & | & | \\ \mathbf{n_1}^{(i),(i+1)} & \mathbf{n_2}^{(i),(i+1)} & \mathbf{n_3}^{(i),(i+1)} \\ | & | & | \end{bmatrix}\begin{bmatrix} \cos(\bar{\omega}) & 0 & \sin(\bar{\omega}) \\ 0 & 1 & 0 \\ -\sin(\bar{\omega}) & 0 & \cos(\bar{\omega}) \end{bmatrix} \tag{14}$$

To facilitate a direct comparison between the closed form solution and the plane scanning method, the same rotation sequence must be utilized (i.e., Eq. (15)).

$$R = R_z(\psi)R_y(\theta) = R_pR_y(\bar{\omega}) = \begin{bmatrix} r_{11} & r_{12} & r_{13} \\ r_{21} & r_{22} & r_{23} \\ r_{31} & r_{32} & r_{33} \end{bmatrix} \tag{15}$$

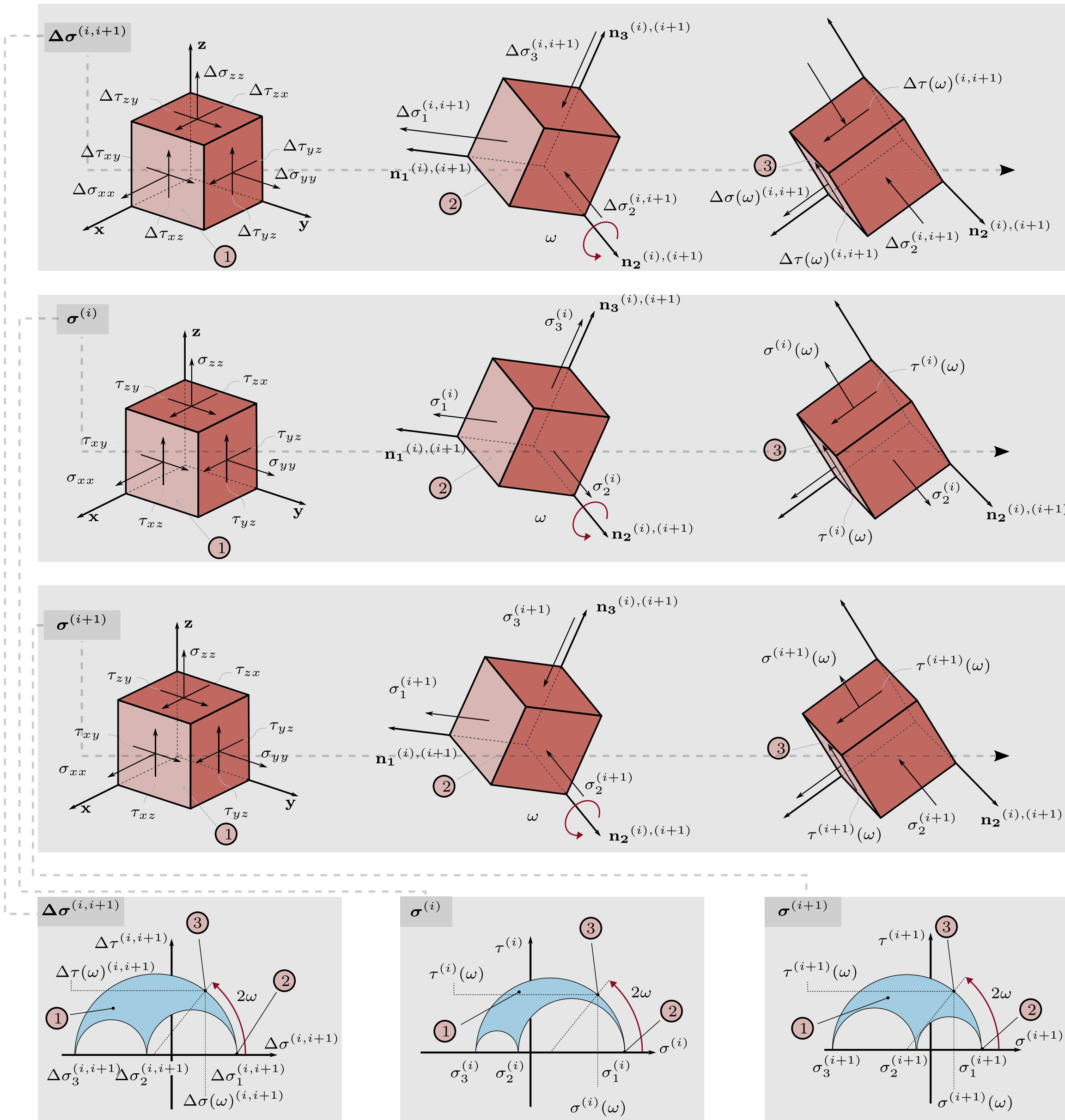

Fig. 2. Graphical representation of the closed form formulation using Cauchy elementary cube and Mohr's circle.

On the basis of Eq. (15), it is now trivial to obtain the two angles (θ and ψ) in analytical form as presented in the following:

1. evaluate all the $\psi_i = \arctan\left(\frac{r_{23}}{r_{13}}\right) + k\pi$ for $k = 1, 2$ in the interval $[0, 2\pi]$;
2. for every ψ_i verify the following condition $\frac{r_{23}}{\sin(\psi_i)}\cos(\psi_i) - r_{13} = 0$;
3. if the condition n. 2 is verified $\psi = \psi_i$ and $\theta = \operatorname{arctan2}\left(\frac{r_{23}}{\sin(\psi_i)}, r_{33}\right)$.

It is worth noting that, in general, two distinct critical plane orientations exist. This assertion holds true in scenarios where the eigenvalues, denoted as $\Delta\sigma_1^{(i,i+1)}$, $\Delta\sigma_2^{(i,i+1)}$, and $\Delta\sigma_3^{(i,i+1)}$, are different from each other. In such a circumstance, a pair of critical planes linked to a common maximum value of the CP parameter FI can be identified, as presented in Fig. 4a. Those planes are identified by the points situated upon the largest Mohr's circle, possessing the same absolute value of the shear stress range value and the same maximum normal stress between the ith and $i+1$th load steps. These planes are obtained by a rotation of $+2\bar{\omega}$ and $-2\bar{\omega}$ about $\mathbf{n_2}$ direction. A special case can be found where one eigenvalue is zero and the other two are opposite, as in case of a fully reversed torsion loading for an axisymmetric specimen. Here two pairs of conjugate critical planes are found by rotating of $\pm\bar{\omega}$ and $\pm(\frac{\pi}{2} - \bar{\omega})$. The reason comes from having the same stress tensors and consequently the same maximum normal stress at the load steps i and $i+1$ as presented in Fig. 4d.

Two distinctive scenarios arise where the analytical formulation either provides partial insights or remains entirely uninformative.

The first case concerns instances where two eigenvalues of $\boldsymbol{\Delta\sigma}$ are identical, as illustrated in Fig. 4b. In this eventuality, an infinite number of critical plane orientations exist, all corresponding to the same FI value. The points characterized within Fig. 4b by angles $\pm 2\bar{\omega}$ can be deduced as an outcome of rotation around the direction (i.e., eigenvector) $\mathbf{n_2}$ or $\mathbf{n_3}$, or any direction that emerges from a linear combination of $\mathbf{n_2}$ and $\mathbf{n_3}$. This implies that all critical planes can be established by rotation about any vector belonging to the plane consisting of $\mathbf{n_2}$ and $\mathbf{n_3}$. An example is provided by an axisymmetric specimen under axisymmetric load conditions.

The second case, as depicted in Fig. 4c, occurs under conditions of a pure hydrostatic stress range state, wherein all three eigenvalues

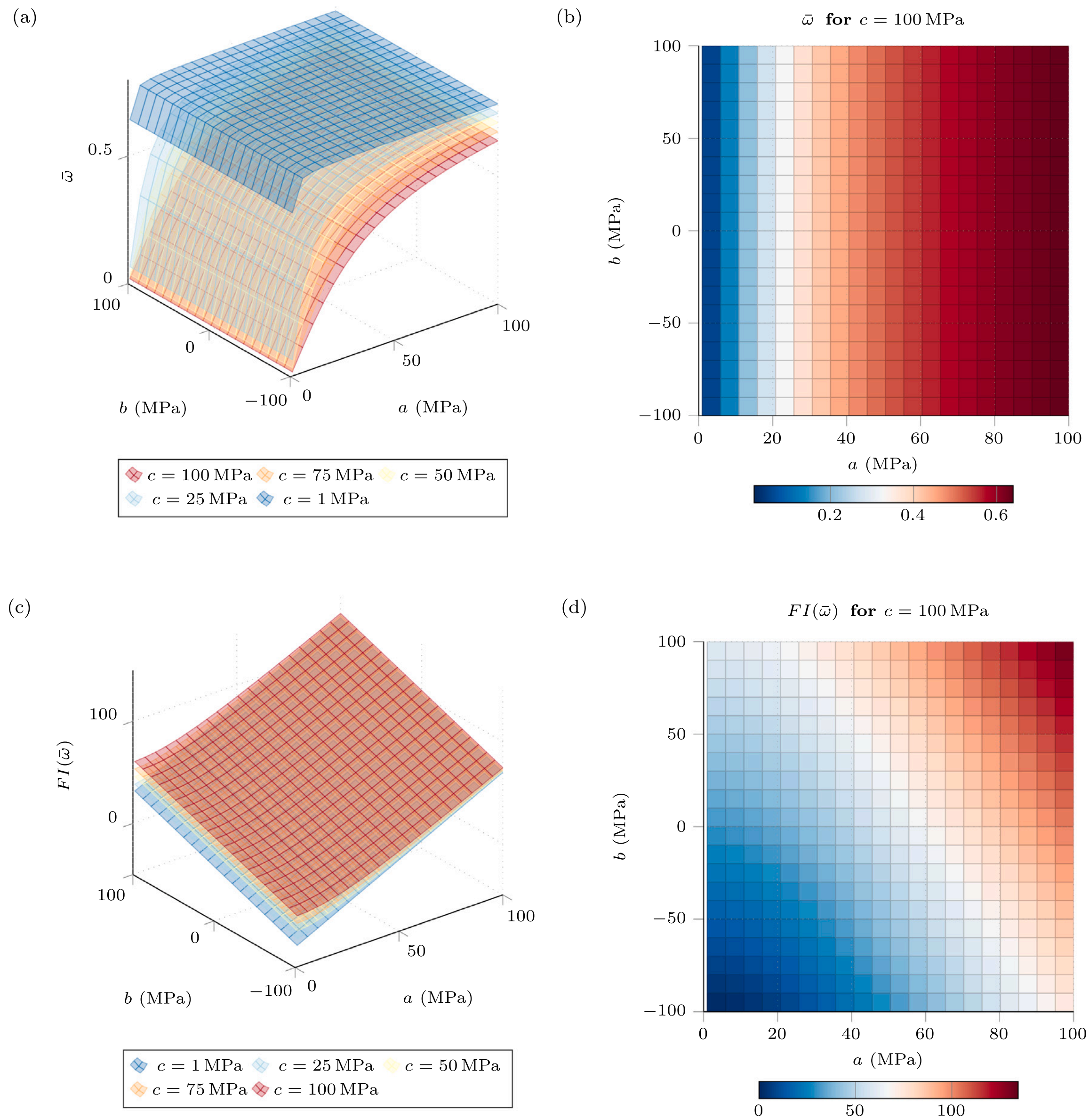

Fig. 3. Surface plots depicting the functions $\bar{\omega}$ and FI are presented as follows: (a) $\bar{\omega}$ over a and b with varying c and for $k = 0.3$, (b) $\bar{\omega}$ over a and b with $c = 100$ MPa and for $k = 0.3$, (c) FI over a and b with varying c and for $k = 0.3$ and (d) FI over a and b with $c = 100$ MPa and for $k = 0.3$.

are identical. In this case the same value of the FI parameter holds for all the orientations; however, this case is not significant for fatigue damage, since, in the considered case of proportional loading, there are no shear stresses in the material.

3. Material and method

In this section, two case studies are presented and analyzed to provide comprehensive and reliable results for a wide range of structural problems. The case studies include a box-welded joint (i.e., as presented by Takahashi et al. (2003) and further studied by Pedersen (2016)) and a tubular specimen (i.e., analyzed by de Freitas et al. (2017)). The box-welded joint was subjected to biaxial tensile–compressive load, while the tubular specimen was subjected to in-phase tension–torsion and pure torsion loading. The components main geometrical parameters are presented in Fig. 5, together with the meshed models and the implemented boundary conditions. Fig. 5a illustrates the box-welded joint, emphasizing the dimensions of the weld seam and the required weld toe radius, which are crucial for the simulation. These values were obtained from the study conducted by Pedersen (2016) and Takahashi et al. (2003).

In order to examine the structural behavior of the box-welded joint and tubular specimen, finite element analyses were conducted using Ansys® software. The analyses focused on the static structural behavior, assuming small displacements and linear elastic material properties characterized by a Young's modulus $E = 210$ GPa and a Poisson's ratio $\nu = 0.3$. Three-dimensional FE-models were developed for both geometries, employing structural brick elements with quadratic shape functions. The mesh size was optimized for each model through convergence analysis, while incorporating symmetries wherever possible. The minimum element dimension, applied specifically in the critical areas, was consistently set at 0.10 mm. It is important to note that the critical area for the box-welded joint was identified at the weld toe on the plate side, while for the tubular specimen, it was located in the region with the smallest thickness.

In order to implement appropriate boundary conditions in the analysis, forces and moments were applied to the red surfaces highlighted in Fig. 5a–b. Similarly, at the blue areas were assigned *fixed support*

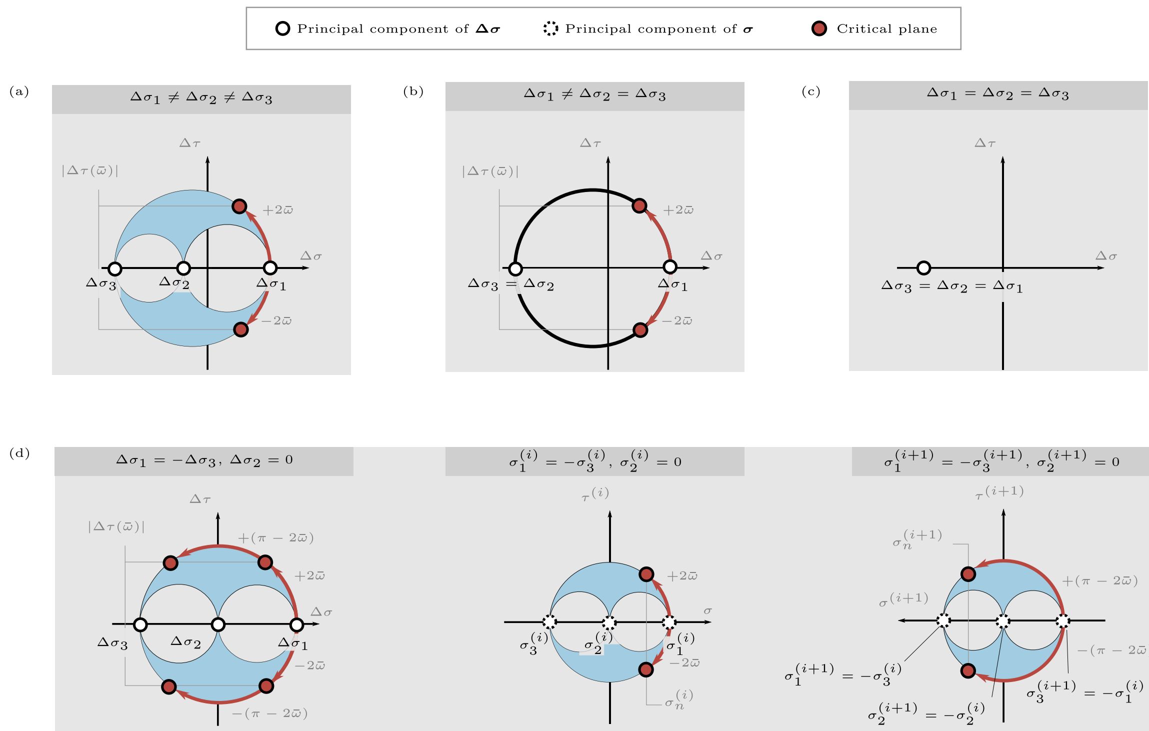

Fig. 4. Representation, by means of the Mohr circles, of the different number of existing critical planes for proportional loading scenarios: (a) all the *eigenvalues* of $\boldsymbol{\Delta\sigma}$ are different, (b) two *eigenvalues* of $\boldsymbol{\Delta\sigma}$ are equal, (c) all the *eigenvalues* of $\boldsymbol{\Delta\sigma}$ are equal and (d) two *eigenvalues* of $\boldsymbol{\Delta\sigma}$ are opposite and one is zero.

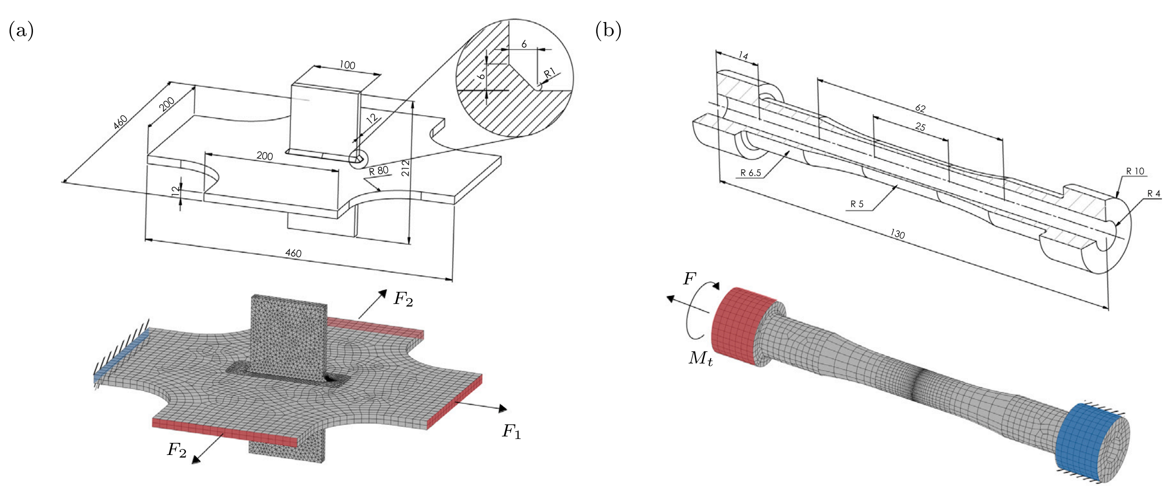

Fig. 5. Main geometrical dimensions and finite element models used in the investigated case studies: (a) box-welded joint and (b) tubular joint. (For interpretation of the references to color in this figure legend, the reader is referred to the web version of this article.)

boundary conditions. Multiple proportional loading sequences were selected, specifically four for the box-welded joint based on the work by Takahashi et al. (2003), and two for the tubular joint based on the research by de Freitas et al. (2017). The loading values, for each case study, are presented in Table 1. The table provides both the magnitudes of the forces and moments, as well as their step-based sequencing implemented in the FE analyses.

4. Results

In this section, the closed-form solution performance in terms of computation time and accuracy of results will be presented. The explicit solutions derived from the functions presented in Section 2.3 yield more precise results compared to numerical approximations (which require convergence analysis). Table 2 displays the results of the *Findley* critical plane coefficient calculated using the closed form formulation and the standard plane scanning method, along with values obtained from the literature. It is noteworthy that the referenced works of Pedersen (2016) and de Freitas et al. (2017) employ slightly different approaches in the computation of FI CP factor. Specifically, Pedersen (2016) utilizes the shear stress range $\Delta\tau$, as the formula reported in Eq. (1), whereas de Freitas et al. (2017) employs the shear stress amplitude $\frac{\Delta\tau}{2}$. This subtle distinction can be readily implemented by adjusting the parameter a of the closed form solution (i.e., considering $\frac{a}{2}$ istead of a).

Table 1
Load steps combination used during simulations with F referring to the applied force and M_t referring to the torque shown in Fig. 5; the graphical overview of the force and moments pattern over load steps is also reported.

Load case	Takahashi et al. (2003)		de Freitas et al. (2017)	
	Load step n.1	Load step n.2	Load step n.1	Load step n.2
Case 1	F_1 = 22.3 kN F_2 = −22.3 kN	F_1 = 464 kN F_2 = −303.5 kN	F = 8.2 kN M_t = 33.6 N m	F = −8.2 kN M_t = −33.6 N m
Case 2	F_1 = 22.3 kN F_2 = −22.3 kN	F_1 = 377.4 kN F_2 = −301.8 kN	F = 0 kN M_t = 43.3 N m	F = 0 kN M_t = −43.3 N m
Case 3	F_1 = 22.3 kN F_2 = −22.3 kN	F_1 = 311 kN F_2 = −301.8 kN	– –	– –
Case 4	F_1 = 22.3 kN F_2 = −22.3 kN	F_1 = 260 kN F_2 = −303.8 kN	– –	– –

Case 1

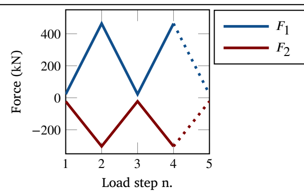

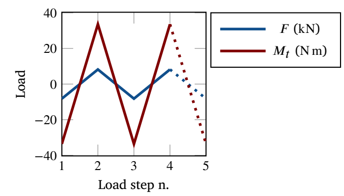

Case 2

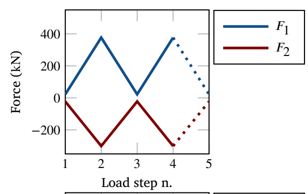

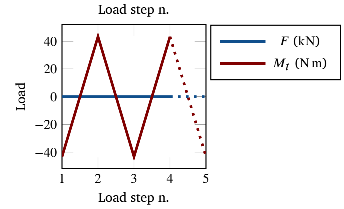

Case 3

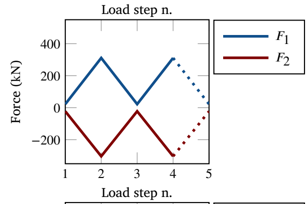

Case 4

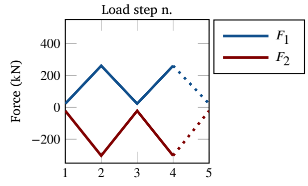

Furthermore, to prove the enhanced computational efficiency, Table 2 provides a comparison of computing times. All code executions were performed using Matlab® on a computer equipped with an 11th Gen Intel(R) Core(TM) i7 processor, 16 GB of RAM, and 4 cores. The performance index (PI) defined in Eq. (16) quantifies the improvement in performance in terms of script evaluation time. A PI value of 100% implies that the computation time for the closed-form solution (t_{cf}) is zero, or alternatively, the computation time for the standard method (t_{ps}) is infinite. Conversely, a PI value of 0% indicates no reduction in computing time. By eliminating the need for multiple plane scanning in space and providing the correct solution, a significant reduction in computing time is achieved. As presented in Table 2, the PI parameter consistently exceeds 99.8%, indicating a substantial improvement in performance.

$$PI = \left(1 - \frac{t_{cf}}{t_{ps}}\right) \tag{16}$$

The implementation of the closed form solution code resulted in a remarkable decrease in computational time from approximately 2 s to around 2×10^{-3} s, for a single node, with a 1° angular step. However, it is expected that a code optimization through the use of lower-level programming languages could lead to additional reductions in computational resources.

Fig. 6 compares the CP orientation and CP values obtained from the two methods for various geometries and loading cases. The comparison is presented graphically to enhance the understanding of the significant improvement achieved by the proposed method. Fig. 6a–b show the results for the in-phase tensile–torsion loading and pure torsion loading for the tubular specimen, while Fig. 6c–f report the biaxial loadings onto the box-welded joint. The CP orientation obtained through the closed form solution is indicated by a white dot in all the figures, and it perfectly matches the maximum values of the colored plots that represent the $FI(\theta, \psi)$ values obtained from spatial plane scanning. The symmetry of the stress tensor along with the loading case, can offer insights into the periodicity of surfaces that exhibit recurring patterns within a specific angular range. It can be noticed in Fig. 6 how the surfaces present a periodicity of π along θ and ψ directions. The solution obtained through the proposed efficient method is inherently unique, however, all infinite solutions can be found using the inherent periodicity of the problem under consideration. The specific values of parameters a, b, and c, necessary to evaluate the closed form solution are provided in Table 3.

Table 2
Comparison of FI values and computational cost between the closed form solution (i.e., cf sol.) and the standard plane scanning method (i.e., ps meth.); literature values of FI (i.e., Pedersen (2016) and de Freitas et al. (2017)) are given for the sake of clarity.

Comparison of *Findley* critical plane factor ($\pm\bar{\omega}$)

Load case	Takahashi et al. (2003)			de Freitas et al. (2017)		
	cf sol.	ps meth.	Pedersen (2016)	cf sol.	sp meth.	de Freitas et al. (2017)
Case 1	523.8 MPa	523.7 MPa	521 ± 3.5 MPa[a]	486.9 MPa	486.9 MPa	488 ± 0.8 MPa[a]
Case 2	440.3 MPa	440.17 MPa	441 ± 3.2 MPa[a]	450 MPa	450 MPa	449.0(6) MPa[a]
Case 3	376.6 MPa	376.5 MPa	375 ± 3.8 MPa[a]	–	–	–
Case 4	328.5 MPa	328.5 MPa	326 ± 3.1 MPa[a]	–	–	–

Comparison of θ and ψ ($+\bar{\omega}$)

	Closed-form		Standard		Closed-form		Standard	
	θ	ψ	θ	ψ	θ	ψ	θ	ψ
Case 1	0.546	0	0.565	0	1.556	0.0612	1.570	0.0628
Case 2	0.547	0	0.565	0	$-1.796 \vert -1.638$[b]	$1.873 \vert 0.286$[b]	$-1.759 \vert -1.633$[b]	$1.884 \vert 0.251$[b]
Case 3	0.549	0	0.565	0	–	–	–	–
Case 4	0.550	0	0.565	0	–	–	–	–

Comparison of θ and ψ ($-\bar{\omega}$)

	Closed-form		Standard		Closed-form		Standard	
	θ	ψ	θ	ψ	θ	ψ	θ	ψ
Case 1	1.810	0	1.822	0	1.367	1.032	1.382	1.005
Case 2	1.808	0	1.822	0	$-1.638 \vert -1.796$[b]	$2.85 \vert 1.268$[b]	$-1.633 \vert -1.759$[b]	$2.82 \vert 1.256$[b]
Case 3	1.807	0	1.822	0	–	–	–	–
Case 4	1.805	0	1.822	0	–	–	–	–

Computational time comparison between cf sol. and ps meth.

	t_{cf}	t_{ps}	PI	t_{cf}	t_{ps}	PI
Case 1	2.24×10^{-3} s	2.14 s	99.89%	2.53×10^{-3} s	2.01 s	99.87%
Case 2	1.973×10^{-3} s	2.45 s	99.91%	2.09×10^{-3} s	2.14 s	99.9%
Case 3	2.35×10^{-3} s	2.39 s	99.91%	–	–	–
Case 4	1.72×10^{-3} s	2.16 s	99.92%	–	–	–

[a] Values derived from the articles (Pedersen, 2016; de Freitas et al., 2017) are represented through a range of variation related to the graphical data acquisition software employed.

[b] The critical plane ($\pm\bar{\omega}$) and its conjugate ($\pm(\frac{\pi}{2} - \bar{\omega})$) are given for the case of pure torsion.

Table 3
Parameter values required to calculate the FI closed-form solution for all case studies described in Fig. 6.

Load case	a (MPa)	b (MPa)	c (MPa)
Case 1 – Takahashi et al. (2003)	382	409	403
Case 2 – Takahashi et al. (2003)	320	346	341
Case 3 – Takahashi et al. (2003)	273	298	294
Case 4 – Takahashi et al. (2003)	237	262	258
Case 1 – de Freitas et al. (2017)	324	145	324
Case 2 – de Freitas et al. (2017)	374	0	374

It is worth noting that if any of the assumptions given in Section 2.3 is not holding, a closed form solution cannot be obtained. Fig. 7 provides a practical example in which a non-proportional loading condition was applied to the tubular specimen, consisting of a first load step with $F = -8.2$ kN and $M_t = 0$ N m and a second load step with $F = 0$ kN and $M_t = -33.6$ N m. Under these conditions a significant difference in FI results can be found both in terms of CP parameter and in terms of the critical plane orientation. Fig. 7 presents the closed form solution compared with the maximum value derived from the standard spatial plane scanning method. For this specific case, an error of 15.72% on the modulus of FI and a maximum error of 0.18 rad on the angular position of the plane is obtained. Then, the application of the closed form solution can be non-conservative when either one of the underlying hypotheses are not met.

5. Conclusions

The objective of this research was to develop a closed form solution for the *Findley* critical plane factor. The method employed the invariants of the stress tensors, as well as the laws of coordinate transformation, and was implemented through a readily available Matlab® script. The closed form solution was discussed and graphically represented using a structural steel as an example, with the potential for similar solutions to be obtained for other metallic materials. A wide range of case studies was analyzed and compared to the standard plane scanning method and to results available in the literature, encompassing various component geometries and loading conditions. Based on the conducted analyses and obtained results, the following conclusions can be drawn:

- the method is applicable for both uniaxial and multiaxial proportional loading conditions, assuming linear-elastic material behavior;
- the method significantly reduces computation time, surpassing a 99.8% reduction compared to the standard plane scanning method for the examined test cases, using a 1° resolution in plane orientation;
- the substantial reduction in computation time enhances the practicality and appeal of using critical plane methods, particularly in industrial contexts with time constraint;
- the proposed method offers a closed-form solution for the *Findley* critical plane and the corresponding damage parameter; the closed-form solution allows a phenomenological interpretation of the critical planes orientation;
- the method is user-friendly and can be implemented in various codes, as it relies on fundamental tensor mathematics; the extension of the method to other critical plane factors appears straightforward.

Reducing computation time during the post-processing phase is vital for evaluating damage factors, as it enables a thorough and comprehensive evaluation of complex models with large numbers of nodes for which the critical locations cannot be easily recognized.

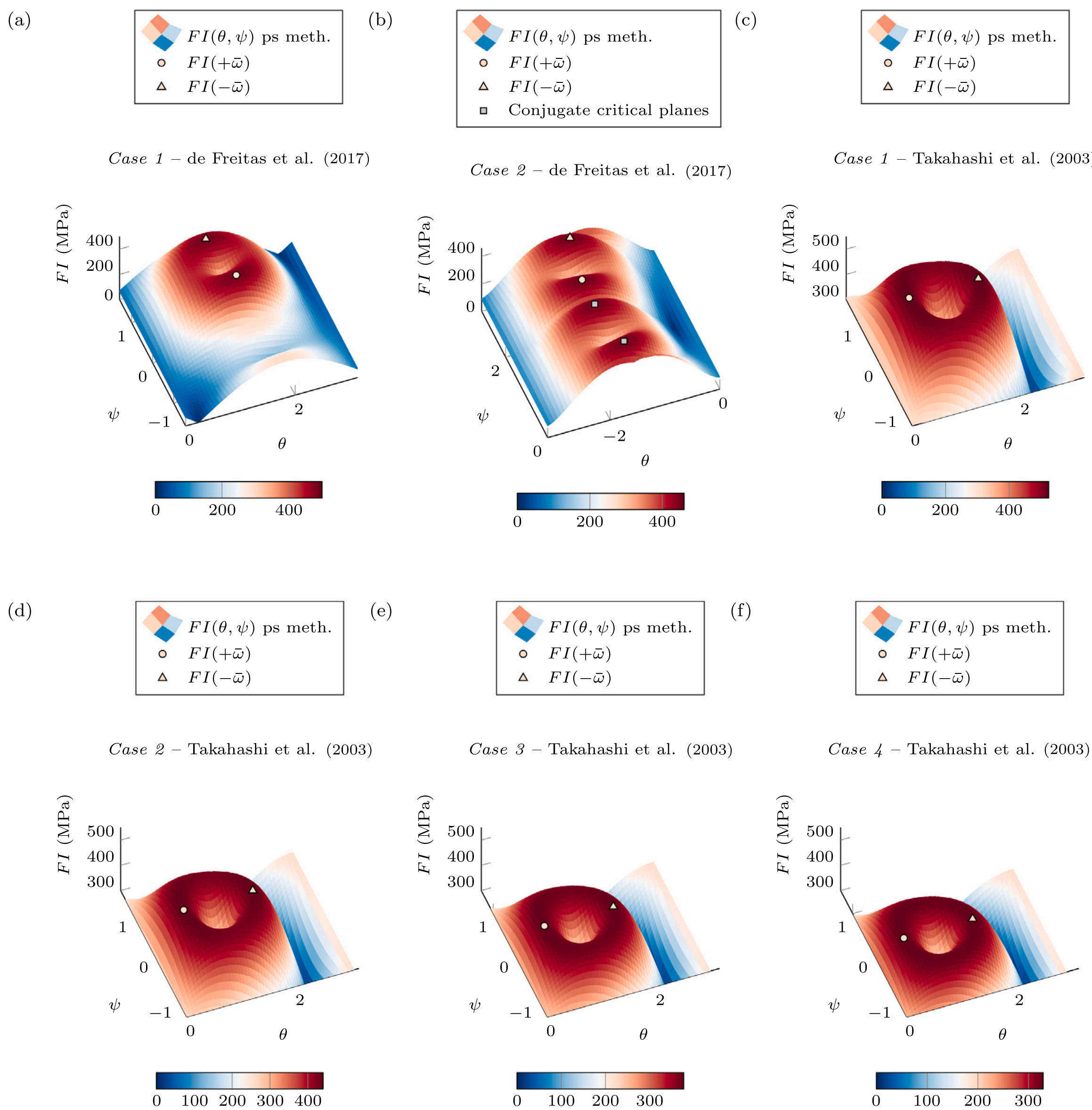

Fig. 6. Comparison of the critical plane factor (FI) solutions obtained from the standard plane scanning method ($FI(\theta,\psi)$ – ps meth.) and the closed-form procedure (FI – cf sol.) for different loading cases: (a) in-phase tension–torsion loading on a tubular specimen, (b) torsion loading on a tubular specimen, (c)–(f) in-phase biaxial loadings on a box-welded joint.

CRediT authorship contribution statement

A. Chiocca: Writing – original draft, Visualization, Software, Methodology, Investigation, Formal analysis, Data curation, Conceptualization. **M. Sgamma:** Writing – review & editing, Validation, Methodology, Investigation, Formal analysis, Conceptualization. **F. Frendo:** Writing – review & editing, Validation, Supervision, Project administration, Funding acquisition, Formal analysis.

Declaration of competing interest

The authors declare the following financial interests/personal relationships which may be considered as potential competing interests: Andrea Chiocca reports financial support was provided by Government of Italy Ministry of Education University and Research.

Data availability

Data will be made available on request.

Acknowledgments

This paper is supported by the Ministry of University and Research (MUR), Italy as part of the PON 2014–2020 "Research and Innovation" resources – Green Action - DM MUR 1062/2021 - Title of the Research: *Sviluppo e riconversione di dispositivi automotive in ottica green: la decarbonizzazione dei veicoli e nuovi impieghi dei sistemi termo-idraulici*.

Appendix A. Supplementary data

A Matlab® script which implements the closed form algorithm reported in the article has been uploaded to a GitHub repository: https://github.com/achiocca1/FI-Sol.

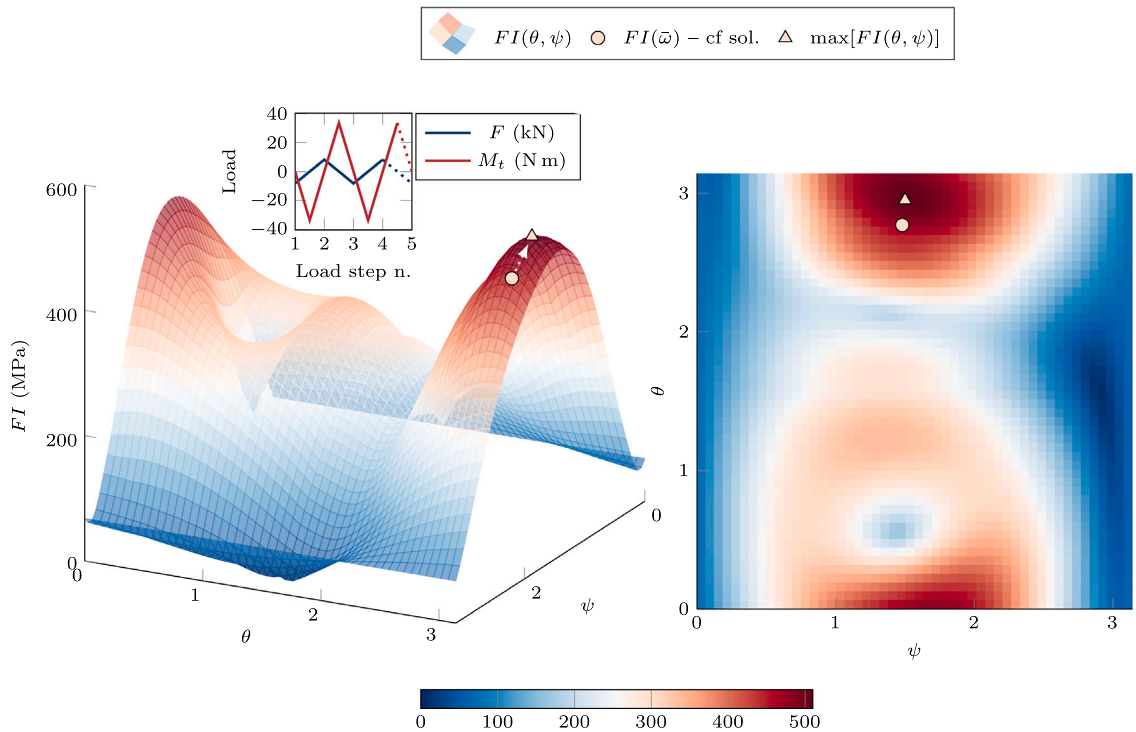

Fig. 7. Comparison of critical plane factor (FI) solutions obtained from the plane scanning method ($FI(\theta,\psi)$) and the closed form solution (FI) for a non-proportional loading case of the tubular specimen.

References

Albinmousa, J., Al Hussain, M., 2021. Polar damage sum concept for constant amplitude proportional and nonproportional multiaxial fatigue analysis. Forces Mech. 4, 100025. http://dx.doi.org/10.1016/j.finmec.2021.100025.

Arora, P., Gupta, S.K., Samal, M.K., Chattopadhyay, J., 2021. Multiaxial fatigue tests under variable strain paths and asynchronous loading and assessment of fatigue life using critical plane models. Int. J. Fatigue 145, 106049. http://dx.doi.org/10.1016/j.ijfatigue.2020.106049.

Berto, F., Lazzarin, P., 2009. The volume-based strain energy density approach applied to static and fatigue strength assessments of notched and welded structures. In: Procedia Engineering. Vol. 1, No longer published by Elsevier, pp. 155–158. http://dx.doi.org/10.1016/j.proeng.2009.06.036.

Bhaumik, S.K., Sujata, M., Venkataswamy, M.A., 2008. Fatigue failure of aircraft components. Eng. Fail. Anal. 15 (6), 675–694. http://dx.doi.org/10.1016/j.engfailanal.2007.10.001.

Braccesi, C., Morettini, G., Cianetti, F., Palmieri, M., 2018. Evaluation of fatigue damage with an energy criterion of simple implementation. In: Procedia Structural Integrity. Vol. 8, Elsevier, pp. 192–203. http://dx.doi.org/10.1016/j.prostr.2017.12.021.

Campagnolo, A., Meneghetti, G., Berto, F., Tanaka, K., 2017. Crack initiation life in notched steel bars under torsional fatigue: Synthesis based on the averaged strain energy density approach. Int. J. Fatigue 100, 563–574. http://dx.doi.org/10.1016/j.ijfatigue.2016.12.022.

Chen, F., Shang, D.-G., Li, D.-H., Wang, L.-W., 2022. Multiaxial thermo-mechanical fatigue life prediction based on notch local stress-strain estimation considering temperature change. Eng. Fract. Mech. 265, 108384. http://dx.doi.org/10.1016/j.engfracmech.2022.108384.

Chiocca, A., Frendo, F., Aiello, F., Bertini, L., 2022. Influence of residual stresses on the fatigue life of welded joints. Numerical simulation and experimental tests. Int. J. Fatigue 162, 106901. http://dx.doi.org/10.1016/j.ijfatigue.2022.106901.

Chiocca, A., Frendo, F., Bertini, L., 2019. Evaluation of residual stresses in a tube-to-plate welded joint. MATEC Web Conf. 300, 19005. http://dx.doi.org/10.1051/matecconf/201930019005.

Chiocca, A., Frendo, F., Bertini, L., 2021. Evaluation of residual stresses in a pipe-to-plate welded joint by means of uncoupled thermal-structural simulation and experimental tests. Int. J. Mech. Sci. 199, 106401. http://dx.doi.org/10.1016/j.ijmecsci.2021.106401.

Chiocca, A., Frendo, F., Marulo, G., 2023a. An efficient algorithm for critical plane factors evaluation. Int. J. Mech. Sci. 242, 107974. http://dx.doi.org/10.1016/j.ijmecsci.2022.107974.

Chiocca, A., Sgamma, M., Frendo, F., 2023b. Closed-form solution for the fatemi-socie extended parameter in case of linear elasticity and proportional loading. Fatigue Fract. Eng. Mater. Struct. http://dx.doi.org/10.1111/FFE.14153.

Chiocca, A., Sgamma, M., Frendo, F., Bucchi, F., 2023c. Rapid and accurate fatigue assessment by an efficient critical plane algorithm: application to a FSAE car rear upright. Procedia Struct. Integr. 47, 749–756. http://dx.doi.org/10.1016/J.PROSTR.2023.07.044.

Chiocca, A., Sgamma, M., Frendo, F., Bucchi, F., Marulo, G., 2024. Fatigue assessment of a FSAE car rear upright by a closed form solution of the critical plane method. Frat. Integr. Strut. 18 (67), 153–162. http://dx.doi.org/10.3221/IGF-ESIS.67.11.

Cruces, A.S., Garcia-Gonzalez, A., Moreno, B., Itoh, T., Lopez-Crespo, P., 2022. Critical plane based method for multiaxial fatigue analysis of 316 stainless steel. Theor. Appl. Fract. Mech. 118, 103273. http://dx.doi.org/10.1016/j.tafmec.2022.103273.

Cruces, A.S., Lopez-Crespo, P., Moreno, B., Antunes, F.V., 2018. Multiaxial fatigue life prediction on S355 structural and offshore steel using the SKS critical plane model. Metals 8 (12), 1060. http://dx.doi.org/10.3390/met8121060.

de Freitas, M., Reis, L., Meggiolaro, M.A., de Castro, J.T.P., 2017. Stress scale factor and critical plane models under multiaxial proportional loading histories. Eng. Fract. Mech. 174, 104–116. http://dx.doi.org/10.1016/j.engfracmech.2016.12.016.

El-sayed, H.M., Lotfy, M., El-din Zohny, H.N., Riad, H.S., 2018. Prediction of fatigue crack initiation life in railheads using finite element analysis. Ain Shams Eng. J. 9 (4), 2329–2342. http://dx.doi.org/10.1016/j.asej.2017.06.003.

European Committee for Standardization (CEN), 2005. Eurocode 3: Design of steel structures — Part 1-9: Fatigue. 50, 77.

Fatemi, A., Socie, D.F., 1988. A critical plane approach to multiaxial fatigue damage including out-of-phase loading. Fatigue Fract. Eng. Mater. Struct. 11 (3), 149–165. http://dx.doi.org/10.1111/j.1460-2695.1988.tb01169.x.

Findley, W.N., 1959. A theory for the effect of mean stress on fatigue of metals under combined torsion and axial load or bending. J. Eng. Ind. 81 (4), 301–305. http://dx.doi.org/10.1115/1.4008327.

Fontana, F., Chiocca, A., Sgamma, M., Bucchi, F., Frendo, F., 2023. Numerical-experimental characterization of the dynamic behavior of PCB for the fatigue analysis of PCBa. Procedia Struct. Integr. 47, 757–764. http://dx.doi.org/10.1016/J.PROSTR.2023.07.043.

Frendo, F., Marulo, G., Chiocca, A., Bertini, L., 2020. Fatigue life assessment of welded joints under sequences of bending and torsion loading blocks of different lengths. Fatigue Fract. Eng. Mater. Struct. 43 (6), 1290–1304. http://dx.doi.org/10.1111/ffe.13223.

Hobbacher, A.F., 2009. The new IIW recommendations for fatigue assessment of welded joints and components - A comprehensive code recently updated. Int. J. Fatigue 31 (1), 50–58. http://dx.doi.org/10.1016/j.ijfatigue.2008.04.002.

Huang, J., Yang, X., Shi, D., Yu, H., Dong, C., Hu, X., 2014. Systematic methodology for high temperature LCF life prediction of smooth and notched Ni-based superalloy with and without dwells. Comput. Mater. Sci. 89, 65–74. http://dx.doi.org/10.1016/j.commatsci.2014.03.023.

Kandil, F.A., Brown, M.W., J., M.K., 1982. Biaxial low-cycle fatigue failure of 316 stainless steel at elevated temperatures. In: Mechanical Behaviour and Nuclear Applications of Stainless Steel at Elevated Temperatures. Maney Pub., London, UK.

Karakaş, Zhang, G., Sonsino, C.M., 2018. Critical distance approach for the fatigue strength assessment of magnesium welded joints in contrast to Neuber's effective stress method. Int. J. Fatigue 112, 21–35. http://dx.doi.org/10.1016/j.ijfatigue.2018.03.004.

Kuncham, E., Sen, S., Kumar, P., Pathak, H., 2022. An online model-based fatigue life prediction approach using extended Kalman filter. Theor. Appl. Fract. Mech. 117, 103143. http://dx.doi.org/10.1016/j.tafmec.2021.103143.

Lazzarin, P., Berto, F., 2005. Some expressions for the strain energy in a finite volume surrounding the root of blunt V-notches. Int. J. Fract. 135 (1–4), 161–185. http://dx.doi.org/10.1007/s10704-005-3943-6.

Liu, J., Ran, Y., Wei, Y., Zhang, Z., 2021. A critical plane-based multiaxial fatigue life prediction method considering the material sensitivity and the shear stress. Int. J. Press. Vessels Pip. 194, 104532. http://dx.doi.org/10.1016/j.ijpvp.2021.104532.

Ma, T.-H., Zhou, C.-Y., Gao, N., Chang, L., He, X.-H., 2022. Low cycle fatigue behavior of CP-Ti under multiaxial load-controlled mode at different multiaxial stress ratios. Int. J. Fatigue 160, 106868. http://dx.doi.org/10.1016/j.ijfatigue.2022.106868.

Marques, J.M.E., Benasciutti, D., Carpinteri, A., Spagnoli, A., 2020. An algorithm for fast critical plane search in computer-aided engineering durability analysis under multiaxial random loadings: Application to the Carpinteri–Spagnoli–Vantadori spectral method. Fatigue Fract. Eng. Mater. Struct. 43 (9), 1978–1993. http://dx.doi.org/10.1111/ffe.13273.

Mirzaei, A.M., Cornetti, P., Sapora, A., 2023. A novel finite fracture mechanics approach to assess the lifetime of notched components. Int. J. Fatigue 173, 107659. http://dx.doi.org/10.1016/j.ijfatigue.2023.107659.

Morettini, G., Braccesi, C., Cianetti, F., Razavi, N., 2021. Design and implementation of new experimental multiaxial random fatigue tests on astm-a105 circular specimens. Int. J. Fatigue 142, 105983. http://dx.doi.org/10.1016/j.ijfatigue.2020.105983.

Morettini, G., Braccesi, C., Cianetti, F., Razavi, N., Solberg, K., Capponi, L., 2020. Collection of experimental data for multiaxial fatigue criteria verification. Fatigue Fract. Eng. Mater. Struct. 43 (1), 162–174. http://dx.doi.org/10.1111/ffe.13101.

Mroziński, S., 2019. Energy-based method of fatigue damage cumulation. Int. J. Fatigue 121, 73–83. http://dx.doi.org/10.1016/j.ijfatigue.2018.12.008.

Pedersen, M.M., 2016. Multiaxial fatigue assessment of welded joints using the notch stress approach. Int. J. Fatigue 83, 269–279. http://dx.doi.org/10.1016/j.ijfatigue.2015.10.021.

Radaj, D., Sonsino, C.M., Fricke, W., 2006. Fatigue Assessment of Welded Joints by Local Approaches: Second Edition. pp. 1–639. http://dx.doi.org/10.1533/9781845691882.

Reis, L., Li, B., De Freitas, M., 2014. A multiaxial fatigue approach to rolling contact fatigue in railways. Int. J. Fatigue 67, 191–202. http://dx.doi.org/10.1016/j.ijfatigue.2014.02.001.

Sgamma, M., Chiocca, A., Bucchi, F., Frendo, F., 2023. Frequency analysis of random fatigue: Setup for an experimental study. Appl. Res. e202200066. http://dx.doi.org/10.1002/appl.202200066.

Sgamma, M., Chiocca, A., Frendo, F., 2024. Rapid and accurate semi-analytical method for the fatigue assessment with critical plane methods under non-proportional loading and material plasticity. Int. J. Fatigue 182, 108191. http://dx.doi.org/10.1016/J.IJFATIGUE.2024.108191, https://linkinghub.elsevier.com/retrieve/pii/S0142112324000495.

Sharma, D., Hiremath, S.S., 2023. Compressive fatigue response of Al-Si10-Mg bionic thin tubes under constant and variable amplitude loading. Int. J. Fatigue 168, 107478. http://dx.doi.org/10.1016/j.ijfatigue.2022.107478.

Socie, D., 1987. Multiaxial fatigue damage models. J. Eng. Mater. Technol. Trans. ASME 109 (4), 293–298. http://dx.doi.org/10.1115/1.3225980.

Sunde, S.L., Berto, F., Haugen, B.r., 2020. Efficient implementation of critical plane for 3D stress histories using triangular elements. Int. J. Fatigue 134, 105448. http://dx.doi.org/10.1016/j.ijfatigue.2019.105448.

Takahashi, I., Takada, A., Ushijima, M., Akiyama, S., 2003. Fatigue behaviour of a box-welded joint under biaxial cyclic loading: Effects of biaxial load range ratio and cyclic compressive loads in the lateral direction. Fatigue Fract. Eng. Mater. Struct. 26 (5), 439–448. http://dx.doi.org/10.1046/j.1460-2695.2003.00645.x.

Tamburrino, F., Chiocca, A., Aruanno, B., Paoli, A., Lardani, L., Carli, E., Derchi, G., Giuca, M.R., Razionale, A.V., Barone, S., 2023. A novel digitized method for the design and additive manufacturing of orthodontic space maintainers. Appl. Sci. 13 (14), 8320. http://dx.doi.org/10.3390/app13148320.

Taylor, D., Barrett, N., Lucano, G., 2002. Some new methods for predicting fatigue in welded joints. Int. J. Fatigue 24 (5), 509–518. http://dx.doi.org/10.1016/S0142-1123(01)00174-8.

Varvani-Farahani, A., Haftchenari, H., Panbechi, M., 2007. An energy-based fatigue damage parameter for off-axis unidirectional FRP composites. Compos. Struct. 79 (3), 381–389. http://dx.doi.org/10.1016/j.compstruct.2006.02.013.

Wang, W.J., Yim, M.S., 2023. A fatigue crack growth prediction model for cracked specimen under variable amplitude loading. Int. J. Fatigue 168, 107387. http://dx.doi.org/10.1016/j.ijfatigue.2022.107387.

Wentingmann, M., Noever-Castelos, P., Balzani, C., 2020. An adaptive algorithm to accelerate the critical plane identification for multiaxial fatigue criteria. In: Proceedings of the 6th European Conference on Computational Mechanics: Solids, Structures and Coupled Problems, ECCM 2018 and 7th European Conference on Computational Fluid Dynamics. ECFD 2018, pp. 3745–3754.